

## Proposed a Mathematical Based Applicable Method for Moho Depth Estimation by Use of Bouguer Anomaly Gravity Data- Case Study

Roshanak Rajablou<sup>1</sup>, Abbas Abbaszadeh Shahri<sup>2</sup> and Fardin Vahidi<sup>3</sup>

<sup>1</sup>Department of Geophysics, Hamedan branch, Islamic Azad University, Hamedan, Iran

<sup>2</sup>Assistant professor, Department of Geophysics, Hamedan branch, Islamic Azad University, Hamedan, Iran

<sup>3</sup>Department of Civil Engineering, University of Guilan, Rasht, Iran

**Corresponding Author:** a\_abbaszadeh@iauh.ac.ir

**Abstract:** At the present study, variation of crustal thickness by Bouguer anomaly gravity and topographic data for the southeast of Iran in the southern part of Kerman province has been investigated. At the first, 2D low-pass filters and upward frequently type analytical techniques were applied to the Bouguer gravity data of the region to inspect the regional gravity anomalies behavior. Then by application of a Moving Window Power Spectrum Method (MWPSM), probable structural depth variations between 32 to 46 km were determined. By applying, the Euler Deconvolution Method (EDM) on Bouguer anomaly gravity data, an investigation of changes in crustal thickness and the type of the anomaly resources was carried out. To validate the proposed method, a comparison between the obtained values with results of Inverted Parker-Oldenburg's Method (IPOM) was conducted. Generation and improvement of a probable 2D crust model by combination of obtained results and proposed seismic velocity models for this region in previous studies was the key factor of this paper.

[Roshanak Rajablou, Abbas Abbaszadeh Shahri and Fardin Vahidi. **Proposed a Mathematical Based Applicable Method for Moho Depth Estimation by Use of Bouguer Anomaly Gravity Data- Case Study.** *Life Sci J* 2012;9(4):5251-5258] (ISSN:1097-8135). <http://www.lifesciencesite.com>. 782

**Keywords:** Crustal thickness, Moving Window Power Spectrum Technique, Euler Deconvolution, Inverted Parker-Oldenburg's Method

### INTRODUCTION

The Power Spectrum Method has used for the determination of crustal thickness using gravity data (Bhattacharyya, 1965 and 1966; Spector and Bhattacharyya, 1966; Jenkis and Watts, 1968; Spector and Grant, 1970; Cianciara and Marcak, 1976; Karner and Watts, 1983; Akgun et al., 1996). By developed MWPSM, a determined profile by windows, which move by certain intervals, can show the depth variations (Cianciara and Marcak, 1976). Euler Deconvolution Method is the other one for estimation of structural parameters. This technique determines the location of the structure, depth and the type of source by using horizontal and vertical derivatives of the anomaly (Thompson, 1982; Reid et al., 1990; Keeting, 1998; Barbosa et al., 1999; Beasley and Golden, 1993; Zhang et al., 2000; Roy et al., 2000; Ozyalin, 2003).

### GEOLOGICAL BACKGROUND OF STUDIED AREA

**Active tectonics:** The northward motion of Arabian with respect to Eurasia, which is shown in figure1, dominates the active tectonics of Iran. At longitude 56° E, ~25 mm/yr of north-south shortening is accommodated across Iran (Sella et al., 2002; McClusky et al., 2003; Vernant et al., 2004a). Several large earthquakes have occurred on the right-lateral strike-slip fault systems along the western margin of the Dasht-e-Lut (Berberian et al., 2001), which accommodate right-lateral shear between central parts of Iran and Afghanistan. However, low rates of seismicity lead the parts of central Iran west of the Dasht-e Lut desert to be considered as relatively strong and non-deforming crustal blocks, in which relatively few active faults have been mapped and relatively few historical earthquakes are recorded (Ambraseys and Melville, 1982). GPS velocities also suggest that the rates of deformation across central Iran are low, at ~3 mm/yr at the longitude of Tehran (Vernant et al., 2004a,b) and at rates of

less than 2 mm/yr at the longitude of Kerman (Vernant et al., 2004b).

**Geology of Kerman province:** The northwest-southeast-trending Kuh-e Bahr Aseman (~3800 m), Kuh Hezar (~4400 m), Kuh-e Lalehzar (~4350 m) and Kuh-e Mamzar (~3100 m) mountain ranges form part of the Sanandaj-Sirjan Tertiary volcanic belt, formed during closure of the Neo-Tethys and subduction of oceanic material (e.g. Stocklin, 1968). The Sanadaj-Sirjan ranges dominate the central part of the study area and separate regions of low relief. We call the northern region the Rafsanjan plain (with an average elevation of ~2000 m to the south of Kuh-e Kalleh Gav and 1600-1700 m to the north of Kuh-e Kalleh Gav) and the southern region the Sirjan plain, again with an elevation of roughly 1700 m. Kuh-e Kalleh Gav and Kuh-e Jupar form isolated ranges within the Rafsanjan plain. Kuh-e Sekonj runs along the eastern boundary of the study area and borders the Gowk right-lateral strike-slip fault (Figs. 1; Berberian et al., 2001). Kuh-e Sekonj and Kuh-e Jupar in the east of the study region consist of conformable Mesozoic and Tertiary sediments. The bedrock geology of northern parts of the Sanandaj-Sirjan zone (south of Anar and in the Kuh-e Kalleh Gav) form a sequence of Cretaceous and early Tertiary turbidite basins (Dimitrijevic, 1973). Rocks exposed within the high ranges of Kuh-e Lalehzar and Kuh-e Hezar are a mixture of unconformable Tertiary sediments and volcanic complexes, with up to 7 km thickness of Eocene volcanics exposed in Kuh-e Bahr Aseman massif (Dimitrijevic, 1973). Thick deposits of Neogene and Quaternary sediment underlie the Rafsanjan and Sirjan plains. The Neogene deposits are typically fine-grained and light-colored marls and sandstones, which are likely to represent the sedimentation before the onset of uplift and faulting. The marls grade upwards into gravels shed from adjacent mountain ranges. The transition to

gravel deposition probably marks the onset of active faulting in the region. The Neogene and Quaternary basin deposits have subsequently been deformed by folding. No detailed information exists on either the stratigraphy or structures developed in the Neogene and Quaternary deposits. Large areas of eastern and central Iran are covered by large late Quaternary alluvial fan surfaces, which are often abandoned and incised by drainage. Although the patterns of river incision may be controlled at the local scale by fault movement, the repeated cycles of deposition and incision within the river system must ultimately be driven by climatic variation within the late Quaternary, as is the case in other parts of central Asia (e.g. Brown et al., 1998; Pan et al., 2003). There is little chronological data to date periods of

alluvial fan deposition in Iran. Figure2 shows a simplified geological map of the studied area.

**APPLIED METHODS**

**Moving Window Power Spectrum Technique:** The accuracy of the spectrum estimation is a statistical approach that depends on the variance and average square error level. In this application, a division on 1D data into equal parts, by window function, is executed and spectrum is obtained separately for divisions. The values in different frequencies are then integrated and their arithmetic mean value is calculated to obtain the spectrum (Jenkins and Watts, 1968). In this method, power spectrum for each division ( $\bar{S}(w)$ ) is given by Cianciara and Marcak (1976) as:

$$\bar{S}(w) = \frac{1}{R} \sum_{r=1}^R \sum_{P=1}^P b_P^r(w, \epsilon_1^{Pr}, \epsilon_2^{Pr}, \dots, \epsilon_n^{Pr}) \exp(-2wh), \tag{1}$$

R: number of divisions, w: angular frequency, h: depth, ε: structure parameter and b: function of anomaly

If, in equation (1), the below inversion is made (Jenkins and Watts, 1968), the equation (2) will appear.

$$b_P^r(w, \epsilon_1^{Pr}, \epsilon_2^{Pr}, \dots, \epsilon_n^{Pr}) = c^{Pr} = \text{constant} \tag{2}$$

$$S = c \cdot \exp(-2wh).$$

By taking the logarithm of equation (2), the average depth of the structure causing anomalies is found as equation (3).

$$\bar{h} = \frac{\ln S(w_{i+1}) - \ln S(w_i)}{2(w_{i+1} - w_i)} \quad i = 1, 2, \dots, \pm N \tag{3}$$

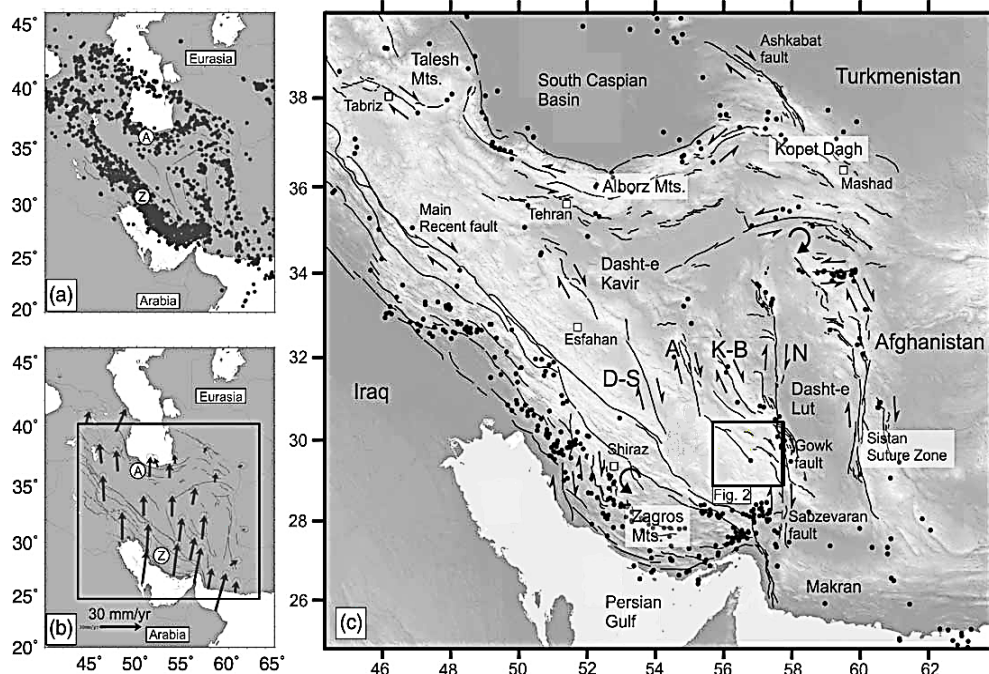


**Figure1.** (a) Instrumentally recorded earthquake epicenters in Iran from the catalogue of Engdahl et al. (1998). (b) A velocity field for Iran determined from repeated GPS measurements (Vernant et al., 2004). Both the seismicity and the deformation measured by GPS are concentrated in central parts of Iran including the selected region (c) Shaded SRTM topography of the studied area showing the major active faults (DehShir (D-S), Anar (A), Kuh-Banan (K-B) and Nayband (N)). The indicated box in geological map represents the studied region that has shown in later figures.

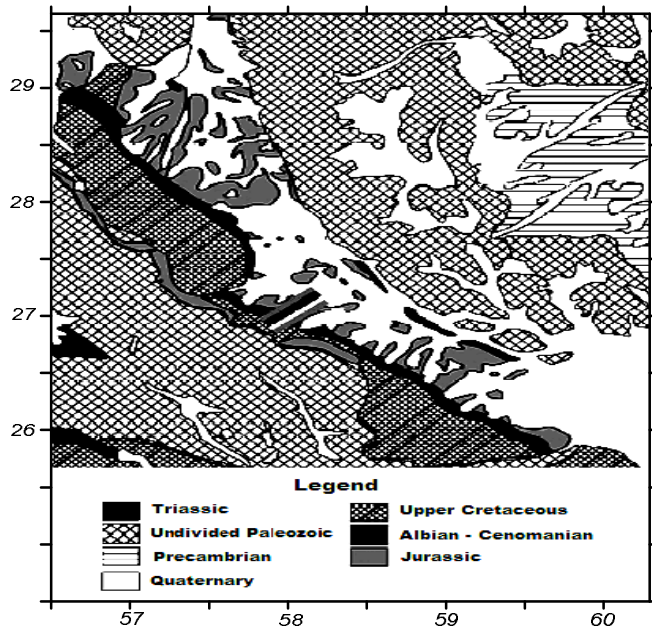


Figure2. Simplified geological map of Kerman province (Hukriede et al., 1962)

2. **Euler Deconvolution Technique:** This technique uses potential field derivatives to image subsurface depth of a magnetic or gravity source (Hsu, 2002). Mushayandebvu et al., (2001) described 2D space Euler's deconvolution equation as given in equation (4).

$$(x - x_0) \frac{\partial T}{\partial x} + (z - z_0) \frac{\partial T}{\partial z} = -N \Delta T \tag{4}$$

( $X_0, Z_0$ ): coordinate position (top of the body),  $Z$ : measured depth as positive down,  $X$ : horizontal distance,  $\Delta T$ : residual field value, and  $N$ : structural index

The structural index is a measure of the variation or fall off rate with field distance and therefore is a function of the causative bodies' geometry. Thus, the magnetic field of a dipole falls off as the inverse cube, giving an index of three, while a vertical line source gives an inverse square field fall off and an index of two. Extended bodies will form assemblages of dipoles and will therefore have indices ranging from zero to three. If  $\Delta T_i$  is the residual field at the  $i^{th}$  point in a magnetic or gravity survey, with the point of measurement at  $(X, Z)$  and the coordinate position of the top of the body  $(X_0, Z_0)$ , then equation (5) can be written as,

$$\begin{bmatrix} \frac{\partial}{\partial x} \Delta T_i & \frac{\partial}{\partial z} \Delta T_i \end{bmatrix} \begin{bmatrix} x - x_0 \\ z - z_0 \end{bmatrix} = N \Delta T_i \tag{5}$$

By calculating the horizontal and vertical gradients of the field, equation (5) has only three unknowns  $X_0, Z_0$  and  $N$ , where the first two describe the location of the body. Many simultaneous equations can be obtained for various measurement locations, which can give rise to one matrix equation.

$$\begin{bmatrix} \frac{\partial}{\partial x} \Delta T_1 & \frac{\partial}{\partial z} \Delta T_1 \\ \frac{\partial}{\partial x} \Delta T_2 & \frac{\partial}{\partial z} \Delta T_2 \\ \vdots & \vdots \end{bmatrix} \begin{bmatrix} x - x_0 \\ z - z_0 \end{bmatrix} = N \begin{bmatrix} \Delta T_1 \\ \Delta T_2 \\ \vdots \end{bmatrix} \tag{6}$$

The least squares method can be used to obtain the unknowns  $X_0$  and  $Z_0$  if the structural index  $N$  is known (Thompson, 1982). Table (1) displays structural indices for different possible geological structures.

Table (1): Structural indices for different geological structures (after Reid et al., 1990)

Structural Index	Geological Structure
0	Contact
0.5	Thick Step
1	Sill / Dike
2	Vertical Pipe
3	Sphere

3. **Parker-Oldenburg's Inversion:** The inversion procedure uses the equation described by Parker (1973) to calculate the gravity anomaly caused by an uneven, uniform layer of material by means of a series of Fourier transforms. This expression, in its one-dimensional form, is defined as:

$$F(\Delta g) = -2\pi\rho G e^{-kz_0} \sum_{n=1}^{\infty} \frac{k^{n-1}}{n!} F[h^n(x)] \tag{7}$$

where  $F(\Delta g)$  is the Fourier transform of the gravity anomaly,  $G$  is the gravitational constant,  $\rho$  is the density contrast across the interface,  $k$  is the wave number,  $h(x)$  is the depth to the interface (positive downwards) and  $z_0$  is the mean depth of the horizontal interface. Oldenburg (1974) rearranged this equation to compute the depth to the undulating interface from the gravity anomaly profile by means of an iterative process and is given by:

$$F[h(x)] = -\frac{F[\Delta g(x)]e^{kz_0}}{2\pi\rho G} \sum_{n=0}^{\infty} \frac{k^{n-1}}{n!} F[h^n(x)] \tag{8}$$

This expression allows us to determine the topography of the interface density by means of an iterative inversion procedure. In this procedure, we assume the mean depth of the interface,  $z_0$ , and the density contrast associated with two media,  $\rho$ . The gravity anomaly is first demeaned prior to the calculation of the Fourier transform. Then, the first term of equation (8) is computed by assigning  $h(x) = 0$  (Oldenburg, 1974) and its inverse Fourier transform provides the first approximation of the topography interface,  $h(x)$ . This value of  $h(x)$  is then used in the equation (8) to evaluate a new estimate of  $h(x)$ . This process is continued until a reasonable solution is achieved. Following Oldenburg (1974), the process is convergent if the depth to the interface is greater than zero and it doesn't intercept the topography. Further, the amplitude of the interface relief should be less than the mean depth of the interface. As the inversion operation (equation 8) is unstable at high frequencies, a high-cut filter, HCF(k) is included in the inversion procedure to ensure convergence of series. This filter is defined by:

$$HCF = \frac{1}{2} \left[ 1 + \cos \left( \frac{k - 2\pi WH}{2(SH - WH)} \right) \right] \tag{9}$$

$$\begin{aligned} WH &= \pi k \pi SH \\ HCF(K) &= 0, k \notin SH \\ HCF(K) &= 1, k \in WH \end{aligned}$$

The mentioned condition is used to restrict the high frequency contents in the Fourier spectrum of the observed gravity anomaly. The frequency,  $k$  can be expressed as  $1/\lambda$ , being  $\lambda$  the wavelength in kilometres. The iterative process is terminated when a certain number of iterations has been accomplished or when the difference between two successive approximations to the topography is lower than a pre-assigned value as the convergence criteria. Once the topographic relief is computed from the inversion procedure, it is desirable to compute the gravity anomaly produced by this computed topography. In general, this modelled anomaly must be very similar to the one used as input at the first step of the inversion process. Estimations of crustal thickness in paper is described with the aid of the flow chart in figure 3.

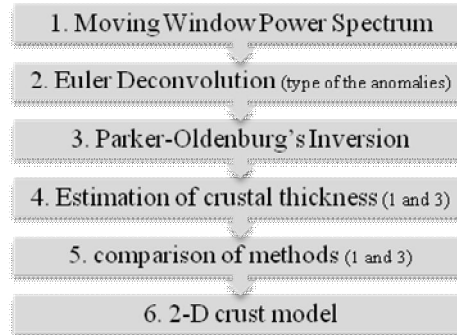


Figure3. Flow chart of various stages in study.

**IMPLEMENTATION**

Bouguer gravity and topographic anomaly maps of Kerman province extending approximately between 57°- 60° E longitudes and 27°- 30° N latitudes with 1-km sampling intervals, which were used at the application stage of this study, were provided by the contribution of the Geological Survey of Iran. When the Bouguer gravity map of Kerman province in figure4 is examined, it can be seen that a regional anomaly with high negative amplitude is dominant. In order to investigate the long-wavelength variation of the high-amplitude anomaly in the region, the two-dimensional low-pass filtering and upward analytic continuation methods were applied to the data as shown in figure5. According to the Airy compensational mechanism, negative anomalies on the bouguer gravity map are interpreted as regions with thick crust and excess mass (mountainous regions) or as hot regions with low density (Hofmann et al., 2006). For this purpose, preceding all, filtering and analytic continuation maps were compared with the topographic map, which has plotted in figure6.

Although the two types of maps seem to be similar in main features, close examination reveals that regions with the same elevations present different Bouguer gravity anomalies. For example, although the section in N-S direction on 58°E longitude on the topographic map in Figure 6 has a topography over 3000 meters, the section giving high amplitude negative anomaly on the filtering map has a boundary between 28.5°-29.5° N latitudes. This shows that the anomaly does not stem only from excess mass and it conveys the presence of another factor. For thoroughly investigating the depths in the region, moving window power spectrum was applied to Bouguer gravity data. The map for probable structural depths in the Kerman province is shown in figure7.

Examination of the obtained depth map (figure7) reveals that the depths in the region range from 32.5 to 45.5 km. In order to estimation the changes within borders of the windows; the Euler deconvolution method was applied to Bouguer gravity data (figure2, profiles A, B) in these profiles (figure8). Examination of the obtained depth map (figure9) reveals that the depths in the region range from 34 to 45.5 km.

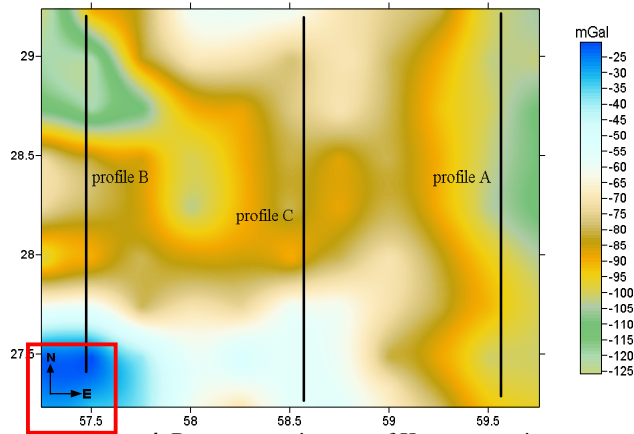


**Figure4.** Bouguer gravity map of Kerman province

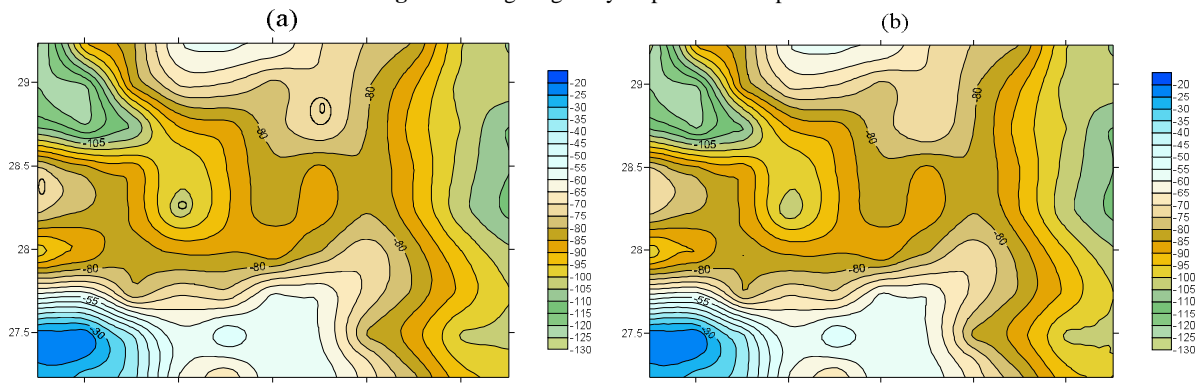


**Figure5. a)** Low-pass filter map of Bouguer gravity data in figure4 **b)** Upward analytic continuation map of Bouguer gravity data in figure4

Examination of the obtained depth map reveals that the depths in the region range from 34 to 45.5 km. From the application of moving windows power spectrum, it was determined that crustal thickness which is ~37.5 km in the south Zagros fault region extends up to ~44 km in the east Sistan suture Zone. And From the application of Parker-Oldenburg's inversion, it was determined that crustal thickness which is ~39 km in the south Zagros fault region extends up to ~44 km in the east Sistan suture Zone which is shown in Table (2).

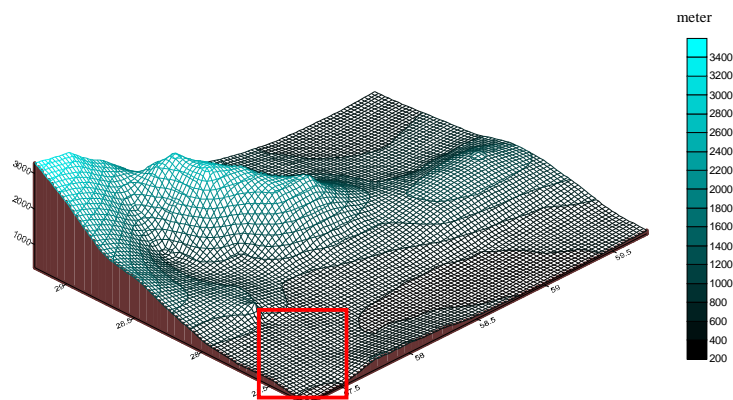


**Figure6.** Topographic maps of the field of study

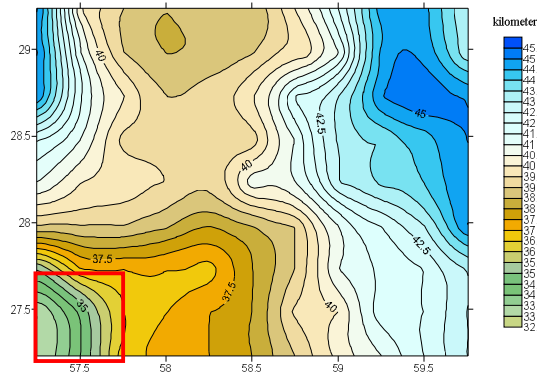


**Figure7.** The map of possible structural depths belonging to the Kerman province obtained from the application of moving window power spectrum method on Bouguer gravity data

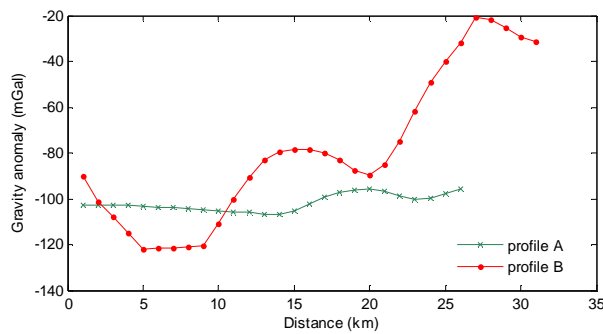


**Figure8.** Values of profiles A, B

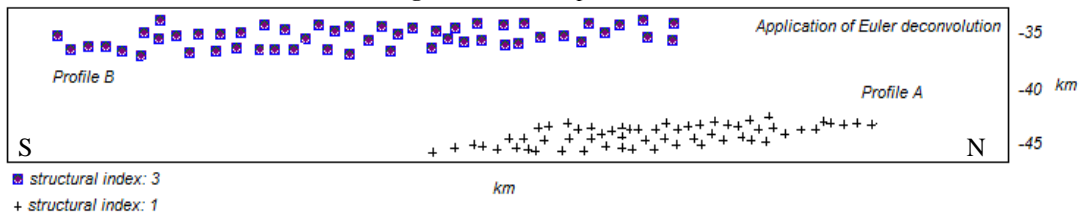


**Figure9.** Application of Euler deconvolution method on Bouguer gravity data of profile A, B in figure8

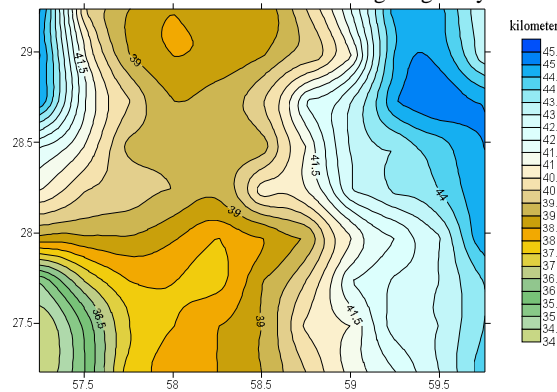


**Figure10.** The map of possible structural depths belonging to the Kerman province obtained from the application of Parker-Oldenburg's inversion on Bouguer gravity data

**Table (2).** Depth values determined from the application of power spectrum method and Parker-Oldenburg's inversion

	Kuh-Banan Fault	Zagros mountains	Gowk fault	Sabzevaran fault
<b>moving window power spectrum</b>	39 (km)	41 (km)	44 (km)	37 (km)
<b>Parker-Oldenburg's inversion</b>	39 (km)	40 (km)	44 (km)	38 (km)

**DISCUSSION AND CONCLUSION**

In this study, using gravity and topographic data from the Kerman province, applications and evaluations have been carried out to determine the variations in crustal thickness. In the first stage, techniques of two-dimensional low-pass filtering and upward analytical continuation were used and behavior of regional gravity anomalies with high negative amplitude in the Kerman province was investigated. After that the moving windows power spectrum method was applied to gravity data; depth estimates were obtained and changes in crustal thickness were examined. In other stage of the application, Euler deconvolution method was applied to Bouguer gravity data, and location and depth of the structure and the type of source were detected. In the last stage, findings obtained from this study, geodynamic processes in the region were examined together with the results of other geophysical and geological studies, and a probable crustal simple model was formed.

Determined thickness by applying the Euler deconvolution method (figure9) pointed the crust thinning begins at nearly 57.5E longitude and continue in the eastern and northern directions. This finding overlaps with those obtained from power spectrum application and Parker-Oldenburg's inversion (figurs7 and 10). Analysis of the Euler deconvolution application provides the solution of the sphere model for the source type causing the anomaly in the western part of the region (figure8, profiles B), and towards the east, it gives the solution of the dike model (figure8, profile A). By application of calculated densities of seismic velocities obtained in the region, Bouguer gravity data belonging to profile C in figure4 were modeled using Talwani et al., (1959) method (figure11). The section where the gravity of the anomaly decreased corresponds to the section where the structural depth is less than expected in particular (The red boxes in figures 4, 6 and 7). Regional anomaly showing high negative amplitude and reaching up to - 125 mgal in the region stems from the low-density zone formed due to high temperatures. The presence of low-velocity layers in a region brings into discussion the concept of low density. Besides the fact that the lithosphere is becoming thin, and the asthenosphere is becoming high causes a decrease in density due to the factor of temperature. These approaches show the presence of low amplitude gravity anomaly. Average depth values determined from the application of power spectrum method and Parker-Oldenburg's inversion in south, north, east and west of Kerman province is shown in Table (2).

Regional anomaly showing high negative amplitude and reaching up to - 125 mgal in the region stems from the low-density zone formed due to high temperatures. Average depth values determined from the application of power spectrum begins from 38 km in the South and reaches 45 km in the East. Moho depth was determined to be changing from 35 to 38 km in sections that present direct correlation between gravity and topographic data according to the Euler deconvolution application. Examination of the lithosphere proposed for the region and the crust-thinning model that comes because of thinning in the lithosphere, support the results obtained from this study.

**REFERENCES**

1. Akgun, M., Akcg, Z., Pinar, R., and Ankaya, O. (1996), Quantitative Interpretation of Self Potential Data by Using of Power Spectra, *Geophysics (in Turkish)* 10, 21–29.
2. Ambraseys, N.N., Melville, C.P., 1982. *A History of Persian Earthquakes*. Cambridge University Press, Cambridge, UK.
3. Barbosa, W., Silva, J.B.C., and Medeiros, W.E. (1999). Stability analysis and improvement of structural index estimation in Euler deconvolution, *Geophysics* 64, 48–60.
4. Beasley, C.W. and Golden, H. C. (1993), Application of Euler deconvolution to magnetic data from the Ashanti belt, southern Ghana: 63rd Ann. Internat. Mtg., Soc. Expl. Geophys., Expanded Abstracts, pg. 417–420.
5. Berberian, M., Baker, C., Fielding, E., Jackson, J.A., Parsons, B.E., Priestley, K., Qorashi, M., Talebian, M., Walker, R., Wright, T.J., 2001. The March 14 1998 Fandoqa earthquake (Mw 6.6) in Kerman province, SEIran: re-rupture of the 1981 Sirch earthquake fault, triggering of slip on adjacent thrusts, and the active tectonics of the Gowk fault zone. *Geophysical Journal International* 146, 371–398.
6. Bhattacharyya, B.K. (1965), Two-dimensional harmonic analysis as a tool for magnetic interpretation, *Geophysics* 30, 829–857.
7. Bhattacharyya, B.K. (1966), Continuous spectrum of the total magnetic field anomaly due to a rectangular prismatic body, *Geophysics* 31, 97–121.
8. Brown, E.T., Bourles, D.L., Raisbeck, G.M., Yiou, F., 1998. Estimation of slip rates in the southern Tien Shan using cosmic ray exposure dates of abandoned alluvial fans. *Geological Society of America Bulletin* 110, 377–386.
9. CIANCIARA, B. and MARCAK, H. (1976), Interpretation of gravity anomalies by means of local power spectra, *Geophys. Prosp.* 24, 273–286.
10. Dimitrijevic, M.D., 1973. *Geology of Kerman Region*. Institute for Geological and Mining Exploration and Investigation of Nuclear and Other Mineral Raw Materials. Report no. Yu/52, 1973, Belgrade.
11. Engdahl, E.R., van der Hilst, R., Buland, R., 1998. Global teleseismic earthquake relocation with improved travel times and procedures for depth determination, *Bulletin of the Seismological Society of America*, 88, 722–743.
12. Hsu Shu-Kun (2002). Imaging magnetic sources using Euler's equation. *Geophysical prospecting*, 50, pp 15–25.
13. Hukriede, R., Kurstem, M. & Venzi aff, H. (1962). *Zur Geologie des gebiets zwischen Kerman und Sagand, Iran*. *Bein. Geol. Jahrb.*, 51.
14. Jenkins, G.M. and Watts, A.B. (1968), *Spectral Analysis and its Applications* (San Francisco: Holden Day).
15. Karner, G.D. and Watts, A.B. (19839), Gravity anomalies and flexure of the lithosphere at mountain ranges. *Geophys. Res.* 88 10449–10477.
16. Keeting, P. B., (1998), Weighted Euler deconvolution of gravity data, *Geophy.* 63, 1595–1603.

17. McClusky, S., Reilinger, R., Mahmoud, S., Ben Sari, D., Tealeb, A., 2003. GPS constraints on Africa (Nubia) and Arabia plate motions. *Geophysical Journal International*, 155, 126–138.
18. Mushayandebvu, M.F., Van Driel, P., Reid, A.B. and Fairhead, J.D. (2001). Magnetic source parameters of two-dimensional structures using extended Euler deconvolution: *Geophysics*, 66, pp 814-823.
19. Oldenburg, D. W., 1974. The inversion and interpretation of gravity anomalies. *Geophysics*, 39(4), 526-536.
20. Ozyalin, S., (2003), Automated interpretation methods in potential fields and application to the archeological sites, Ph.D. Thesis, DokuzEylu" I Univ. Grad. School of Natural and Appl. Sci. Izmir Turkey, 271 (in Turkish).
21. Pan, B., Burbank, D., Wang, Y., Wu, G., Li, J., Guan, Q., 2003. A 900 k.y.record of strath terrace formation during glacial–interglacial transitions in northwest China. *Geology* 31, 957–960.
22. Parker, R. L., 1973. The Rapid Calculation of Potential Anomalies. *Geophysical Journal of the Royal Astronomical Society*, 31, 447-455.
23. Reid, A. B., Allsop, J. M., Granser, H., Millett, A. J., and Somerton, I. W., (1990), Magnetic interpretation in three dimensions using Euler deconvolution: *Geophysics*, 80–91.
24. Roy, L., Agarwal, B.N.P., and Shaw, R.K. (2000), A new concept in Euler deconvolution of isolated gravity anomalies. *Geophy. Prospecting* 48, 559–575.
25. Sella, G.F., Dixon, T.H., Mao, A., 2002. REVEL: a model for recent plate velocities from space geodesy. *Journal of Geophysical Research* 107. doi:10.1029/2000JB000033.
26. SPECTOR, A. and BHATTACHARYYA, B.K. (1966), Energy spectrum and auto correlation functions of anomalies dueto dikes; the complex gradient method, *Geophys.*46, 1572–1578.
27. SPECTOR, A. and GRANT, F.S. (1970), Statistical models for interpreting aeromagnetic data, *Geophys.* 35,242–272.
28. Stocklin, J., 1968. Structural history and tectonics of Iran: a review, *Bulletin of the American Association of Petroleum Geologists*, 52, 1229–1258.
29. Talwani, M., Wo"RZEL, J.L., and LANDISMAN, M. (1959), Rapid gravity computations for two dimensional bodies with application to the Mendocino Submarine Fracture Zone. *Jo. Geophys. Res.* 64, 49 59.
30. Thompson, D.T. (1982), EULDPH-A technique for making computer–assisted depth estimates from magnetic data, *Geophys.* 47, 31–37.
31. Vernant, Ph., Nilfroushan, F., Hatzfeld, D., Abbassi, M.R., Vigny, C., Masson, F., Nanakali, H., Martinod, J., Ashtiani, A., Bayer, R., Tavakoli, F., Chery, J., 2004a. Contemporary crustal deformation and plate kinematics in Middle East constrained by GPS measurements in Iran and northern Oman. *Geophysical Journal International* 157, 381–398.
32. 381–398.
33. Vernant, Ph., Nilfroushan, F., Chery, J., Bayer, R., Djamour, Y., Masson, F., Ritz, J.-F., Sedighi, M., Tavakoli, F., 2004b. Deciphering oblique shortening of central Alborz in Iran using geodetic data. *Earth and Planetary Science Letters* 223, 177–185.
34. Zhang, C., Mushayandebvu, M.F., Reid, A.B., Fairhead, J.D., and Odegard, M.E. (2000), Euler deconvolution of gravity tensor gradient data, *Geophys.* 65, 512–520.